Journal of Alloys and Compounds 500 (2010) 206–210

Contents lists available at ScienceDirect

Journal of Alloys and Compounds

journal homepage: www.elsevier.com/locate/jallcom

Investigation on magnetic properties of α-Fe_2O_3 nanoparticles synthesized under surfactant-free condition by hydrothermal process

Manish Srivastava[a], Animesh K. Ojha[b,*,1], S. Chaubey[a], Jay Singh[c], Prashant K. Sharma[d], Avinash C. Pandey[d]

[a] Department of Physics, Motilal Nehru National Institute of Technology, Allahabad, Allahabad 211004, India
[b] School of Engineering and Science, Jacobs University, 28759 Bremen, Germany
[c] Department of Chemistry, Motilal Nehru National Institute of Technology, Allahabad, Allahabad 211004, India
[d] Nanophosphor Application Centre, University of Allahabad, Allahabad 211002, India

ARTICLE INFO

Article history:
Received 17 March 2010
Accepted 31 March 2010
Available online 8 April 2010

Keywords:
Iron oxide
Hydrothermal
TEM
Magnetic properties

ABSTRACT

Impurity free α-Fe_2O_3 nanoparticles have been synthesized by hydrothermal method using two different precursors, $FeCl_3 \cdot 6H_2O$ and $Fe(NO_3)_3 \cdot 9H_2O$. The physical properties of the synthesized nanoparticles were investigated by X-ray diffraction (XRD), Raman spectroscopy (RS), scanning electron microscope (SEM) high resolution transmission electron microscope (HR-TEM) and vibrating sample magnetometer (VSM). The average particle size of the nanoparticles synthesized using $FeCl_3 \cdot 6H_2O$ and $Fe(NO_3)_3 \cdot 9H_2O$ was calculated to be ~60 and ~87 nm, respectively. The magnetic properties of the α-Fe_2O_3 nanoparticles synthesized using both the precursors were found be quite different, which may be attributed to the different particle size of the nanoparticles.

1. Introduction

For last few decades, the studies on nanomaterials have been enhanced by the research community due to its diverse range of applications such as magnetic storage media, environment protection, sensors, catalysis, clinical diagnosis and treatment [1–2]. In most of the studies the emphasis has been given to synthesis and characterization of nanomaterials, which have the capability to exhibit certain superior properties as compared to their bulk form. Among the various types of nanomaterials, the magnetic materials of iron oxides such as α-Fe_2O_3 and Fe_3O_4 are the most popular and promising materials due their many technological applications. The selection of right materials as the precursor for the synthesis of iron oxide nanoparticles is a crucial task. The many forms of iron oxides such as Fe_3O_4, γ-Fe_2O_3 and α-Fe_2O_3 can be synthesized by varying the synthesis conditions. The precipitation of the aqueous Fe^{2+}/Fe^{3+} solution [3] or in situ generated Fe^{3+} solution [4] make to form Fe_3O_4 and γ-Fe_2O_3 nanoparticles. However, the synthesis under high temperature results α-Fe_2O_3 nanoparticles [5]. Ferromagnetic nanoparticles can also be synthesized through the hematite route owing to the higher stability of hematite and then subsequently reduced to magnetite [6]. Highly ordered nanoparticles of magnetite have been synthesized using trypsin as a template [7]. Along with the antiferromagnetic nature, the α-Fe_2O_3 nanoparticle has very good semiconducting properties with a band gap of 2.1 eV. It is more stable [8], offer high resistance to corrosion [9] and nontoxic. Therefore, it is a good choice for the technological applications. It has been widely used as gas sensing material [10–12], heterogeneous catalyst [13], photocatalyst [14] and pigments [15] and its nanowires form excellent anodes for electrolysis of water [16].

To exploit the interesting and useful properties of nanostructures and to incorporate them into technology, their controlled and well dispersed synthesis is quite essential. The synthesis of monodispersed α-Fe_2O_3 nanoparticles with various structural morphologies have attracted much interest due to their importance to have a thorough understanding of several fundamental phenomenon such as light scattering, particle interaction and electrophoresis. Up to now, several synthesis methods have been developed for the preparation of α-Fe_2O_3 nanoparticles which include sol–gel, hydrolysis of iron salt and hydrothermal synthesis. The hydrothermal synthesis process has proven to be advantageous over other methods due to the presence of homogeneous nucleation and grain growth. In addition to synthesis of well disperse and homogeneous nanoparticles, the hydrothermal method can also be realized to have less impurity in the synthesized products using a low processing temperature such as 200 °C or even less [17–18].

* Corresponding author. Tel.: +91 5322771289; fax: +91 532 2545341.
E-mail addresses: animesh@mnnit.ac.in, animesh_r1776@rediffmail.com (A.K. Ojha).
[1] On leave from the Department of Physics, Motilal Nehru National Institute of Technology, Allahabad 211004, India.

0925-8388/$ – see front matter © 2010 Elsevier B.V. All rights reserved.
doi:10.1016/j.jallcom.2010.03.245

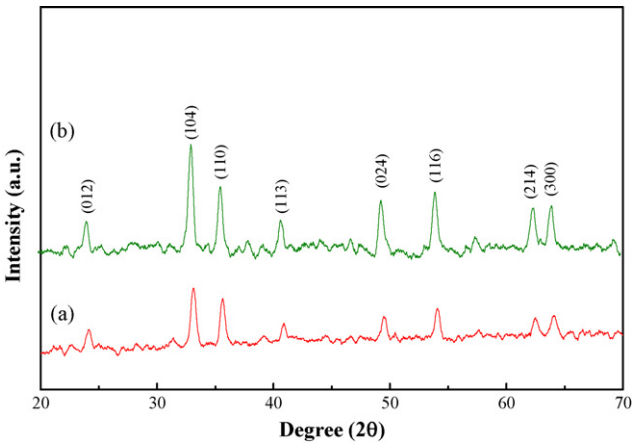

Fig. 1. XRD pattern of α-Fe_2O_3 nanoparticles synthesized by ferric nitrate (a) and ferric chloride (b) as the precursors.

Table 1
Lattice parameters and particles size of the α-Fe_2O_3 nanoparticles synthesized by two different iron precursors.

Precursor	Lattice parameter (Å)	Particles size (nm) calculated by distribution curve
$Fe(NO_3)_3{\cdot}9H_2O$	$a = b = 5.0354$, $c = 13.746$	~87
$FeCl_3{\cdot}6H_2O$	$a = b = 5.0352$, $c = 13.743$	~60

In view of the above mentioned studies on the synthesis and characterizations of α-Fe_2O_3 nanoparticles and its derivatives, and also its wide application, it was thought worthwhile to synthesize highly ordered and monodisperse α-Fe_2O_3 nanoparticles through a relatively simple and low cost method. Although, the various types of α-Fe_2O_3 nanostructures have been successfully synthesized via different synthesis methods but the synthesis of monodisperse α-Fe_2O_3 nanoparticles have been rarely found in the literature. Thus in the present study we have successfully synthesized monodisperse α-Fe_2O_3 nanoparticles through hydrothermal method using two different precursors of iron $Fe(NO_3)_3{\cdot}9H_2O$ and $FeCl_3{\cdot}6H_2O$ under a surfactant-free environment. The synthesized α-Fe_2O_3 was characterized through different experimental techniques for exploring their particle nature and other physical properties. In addition to this we have also investigated the effect of two iron precursors on the physical properties of the α-Fe_2O_3 nanoparticles. Thus the present study is expected to give a detailed overview of the synthesis and physical properties of monodisperse α-Fe_2O_3 nanoparticles.

2. Experimental

2.1. Preparation of samples

The well disperse α-Fe_2O_3 nanoparticles were synthesized via hydrothermal method at 180 °C using $Fe(NO_3)_3{\cdot}9H_2O$ and $FeCl_3{\cdot}6H_2O$ as two different iron precursors. The 25% aqueous solution of ammonia was used as a mineralizer. The details of the synthesis procedure adopted in the preset study are as follows. At first, two different aqueous solutions of high-purity $Fe(NO_3)_3{\cdot}9H_2O$ and $FeCl_3{\cdot}6H_2O$ were prepared in de-ionized water to form a uniform solution by stirring. Subsequently, 25% aqueous solution of ammonia was slowly dropped into the above two different solutions under constant-rate stirring and the pH value of the solutions was adjusted to ~8.0. The resulted solutions were vigorously stirred and then poured into two different Teflon vessels until 3/4th of its total volume capacity and then the vessel was placed in a stainless steel tank to perform the hydrothermal treatment at 180 °C for 24 h. Once the reaction gets over, the autoclave was put separately to bring down its temperature. Further, we wait till the autoclave was cooled down to room temperature naturally. The obtained products were washed several times with distilled water and dried at 40 °C for 12 h. Finally, a brown powder was obtained.

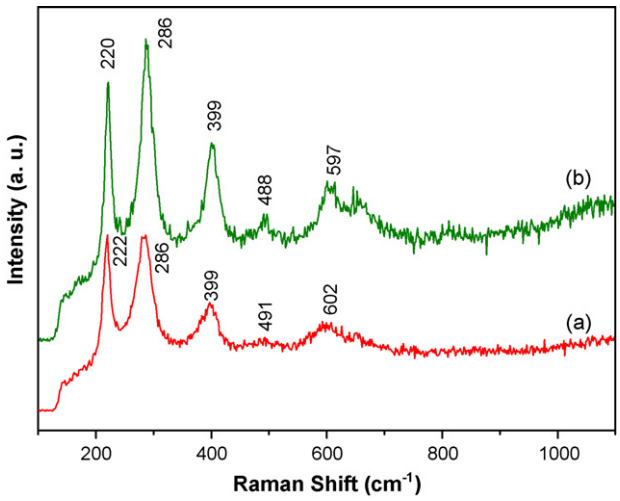

Fig. 2. Raman spectra of α-Fe_2O_3 nanoparticles synthesized by ferric nitrate (a) and ferric chloride (b) as the precursors.

2.2. Characterization techniques

The crystallographic study of the synthesized product was performed using powder XRD XPERT-PRO (PW3050/60) equipped with Cu-Kα radiation (λ = 1.54060 Å) operated at 30 kV and 30 mA. The room temperature Raman spec-

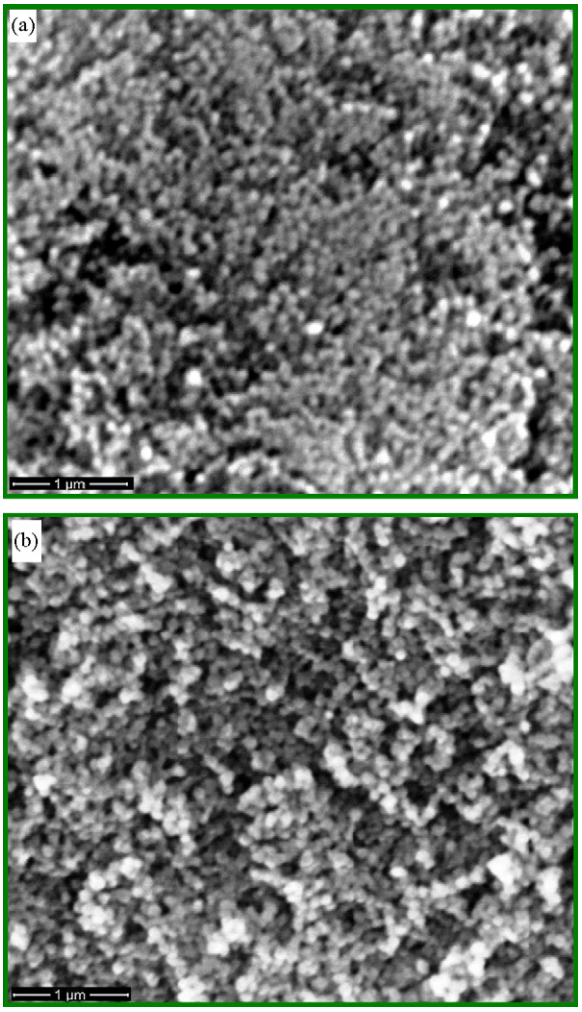

Fig. 3. SEM micrograph of α-Fe_2O_3 nanoparticles synthesized by ferric nitrate (a) and ferric chloride (b) as the precursor.

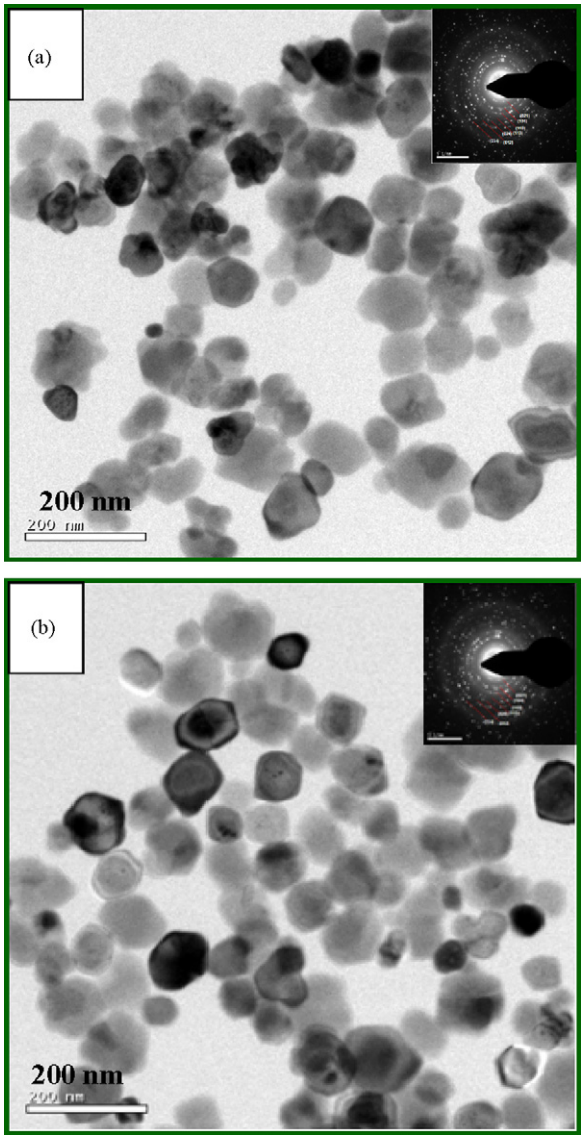

Fig. 4. TEM micrograph and (SAED in the inset bar length is 5 1/nm) pattern of α-Fe_2O_3 nanoparticles synthesized by ferric nitrate (a) and ferric chloride (b) as the precursor.

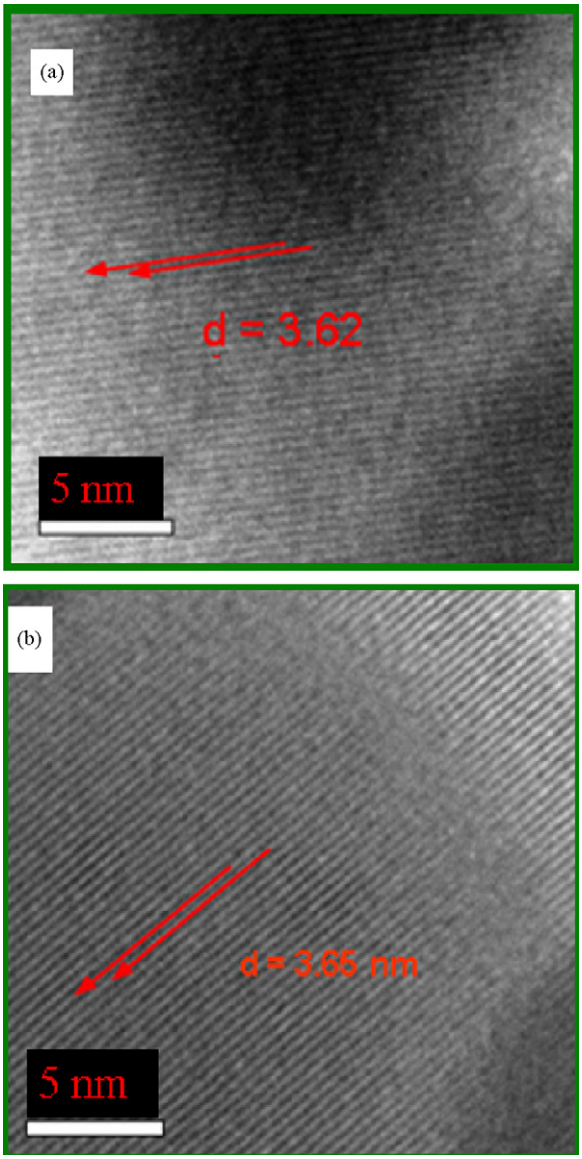

Fig. 5. HR-TEM image of the α-Fe_2O_3 nanoparticles synthesized by ferric nitrate (a) and ferric chloride (b) as the precursor.

tra were recorded in the range of 200–1200 cm^{-1} using a Renishaw invia Raman spectrometer equipped with a high-performance CCD detector. The 514 nm line of Argon-ion laser was used to illuminate the sample (FEI QUANTA-200 MK2). The structural morphology and the particles size were investigated by SEM and HR-TEM (TEM, Tecnai F30). The hysteresis loop, saturation magnetization (Ms) and coercivity (Hc) of the α-Fe_2O_3 nanoparticles were also measured by means of VSM at a maximum applied field of 17,500 Oe at room temperature.

3. Results and discussion

3.1. Structural characterization

Fig. 1 shows the XRD patterns of the synthesized products derived from hydrothermal method. Both the products were indexed as pure α-Fe_2O_3 with rhombohedral structure. The diffraction peaks of both the samples corresponding to (0 1 2), (0 1 4), (1 1 0), (1 1 3), (0 2 4), (1 1 6), (2 1 4) and (3 0 0) planes are in good agreement with the standard XRD pattern of α-Fe_2O_3 derived from the JCPDS Card No. 33-664 [19]. The average particle size (D_{hkl}) was calculated by using the following Debye–Scherrer equation [20]:

$$D = \frac{0.9\lambda}{\beta \cos\theta} \quad (1)$$

where λ is the wavelength of the target Cu-Kα 1.54060 Å, β is the full width at half maximum (FWHM) corresponding to the most intense diffracted peak corresponding to (3 1 1) plane. The size of the α-Fe_2O_3 nanoparticles synthesized using $Fe(NO_3)_3{\cdot}9H_2O$ and $FeCl_3{\cdot}6H_2O$ as the precursors were found to be ~60 and ~50 nm, respectively The calculated lattice constants are shown in Table 1.

3.2. Raman study of the α-Fe_2O_3 nanoparticles

Hematite belongs to the D^6_{3d} crystal space group. Thus, seven Raman bands are expected to appear in the Raman spectra of the material [21]. These seven bands are belonging to mainly; two A_{1g} symmetry species, 221 and 498 cm^{-1} and five E_g symmetry species, 244, ~290, ~298, ~401 and 605 cm^{-1}. The room temperature Raman spectra of synthesized α-Fe_2O_3 nanoparticles

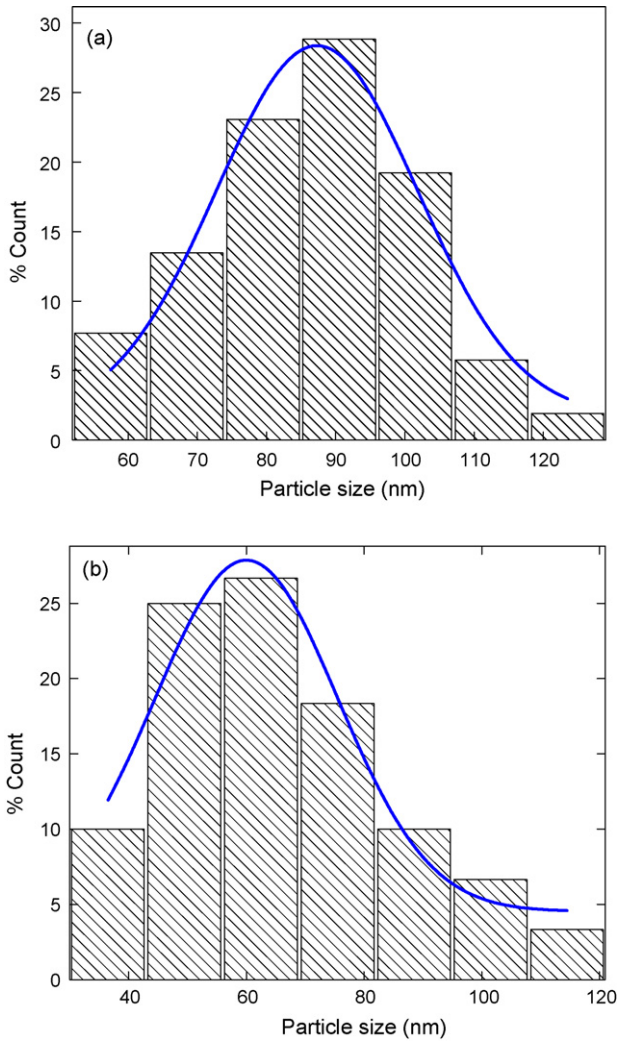

Fig. 6. Size distribution histograms and Gaussian fits for α-Fe_2O_3 nanoparticles synthesized by ferric nitrate (a) and ferric chloride (b) as the precursor.

recorded in the range, 200–1200 cm^{-1} are shown in Fig. 2. The Raman bands appeared in the spectral range, 290–298 cm^{-1} are usually reported as a doublet of E_{1g} symmetry and cannot be easily resolved. No unambiguous signal from other iron oxide phases was observed in the Raman spectra. In the present study some differences in the position of Raman vibrational modes were observed in comparison to the earlier study on α-Fe_2O_3 nanowires [22]. This could be explained in terms of particle and rod type nature of electron confinement in the synthesized α-Fe_2O_3 nanostructure, which essentially affect the phonon modes and thus the Raman shift.

3.3. SEM/HR-TEM/SAED analysis of the α-Fe_2O_3 nanoparticles

The crystallinity, particle size and structural morphology of the synthesized α-Fe_2O_3 nanoparticles were further characterized with SEM, TEM, HR-TEM and SAED as shown in Figs. 3–5. SEM micrograph of the α-Fe_2O_3 nanoparticles shows that particles are uniformly distributed. The TEM images of the nanoparticles reveal that the particles have both, hexagonal and spherical morphologies along with the monodisperse in nature. The size of α-Fe_2O_3 nanoparticles synthesized by taking both, $Fe(NO_3)_3{\cdot}9H_2O$ and $FeCl_3{\cdot}6H_2O$ as the precursors were observed to be in the range of 30–120 nm. The selected area electron diffraction (SAED) pattern (see inset of Fig. 4(a) and (b)) taken from the whole area of the nanoparticles turned out to be a series of diffraction rings with bright spots, which may be attributed to the polycrystalline nature of the synthesized nanoparticles [23]. Every diffraction ring could be well indexed to the corresponding crystal planes of hematite, which essentially confirms that the synthesized nanoparticles are α-Fe_2O_3 [24,25]. Further, to confirm the growth direction a nanoparticle was selected for HR-TEM study. Fig. 5(a) and (b) shows the clearly resolved lattice spacing of 3.62 and 3.65 Å, which correspond to the (2 1 0) plane.

Table 2
Magnetic properties such as Ms, Mr and Hc of the α-Fe_2O_3 nanoparticles synthesized by two different iron precursors.

Precursor	Saturation magnetization (Ms) (emu/g)	Remanent magnetization (Mr) (emu/g)	Coercivity (Hc) (Oe)
$Fe(NO_3)_3{\cdot}9H_2O$	0.573	0.100	589.0
$FeCl_3{\cdot}6H_2O$	0.340	0.016	303.0

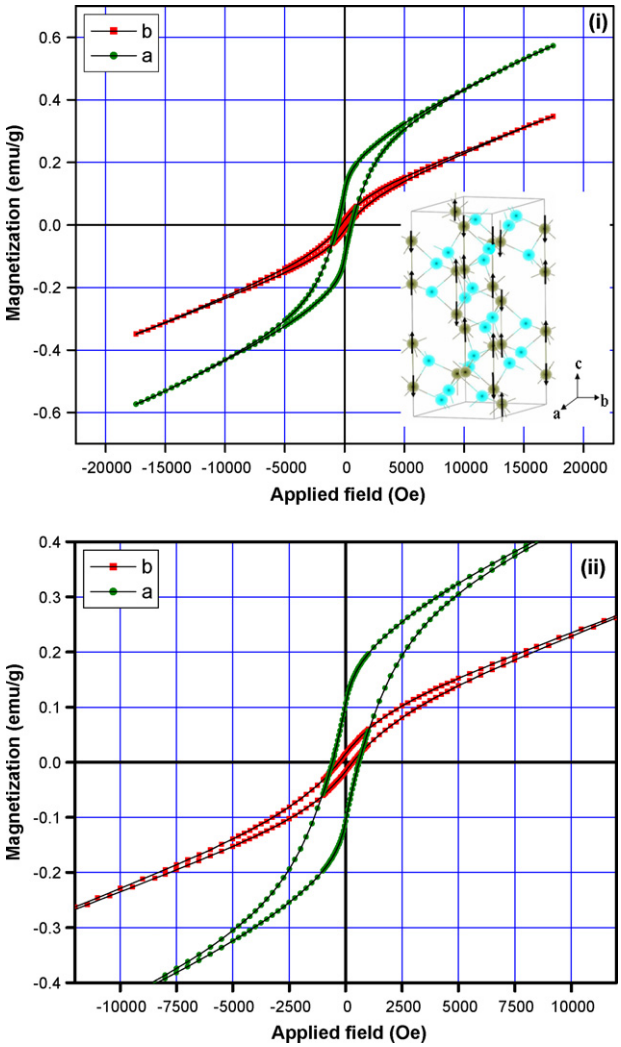

Fig. 7. (i) Hysteresis loop of α-Fe_2O_3 nanoparticles synthesized by ferric nitrate (a) and ferric chloride as the precursors (b) at the applied field of 17.5 kOe and the figure in the right corner is the structure of hematite (α-Fe_2O_3) in the hexagonal setting with vectors indicating spin directions (ii) hysteresis loop of α-Fe_2O_3 nanoparticles at the applied filed of 12 kOe.

3.4. Particle size distribution

The distribution of the particles size obtained through the TEM micrograph is shown in Fig. 6(a) and (b). In order to analyze the size distribution quantitatively, the particle size distribution was fitted as Gaussian function [26]:

$$P(D) = \frac{A}{\sqrt{2\pi\sigma_D}} \exp\left\{-\frac{(D - D_m)^2}{2\sigma_D^2}\right\}$$

where σ_D is the standard deviation of the diameter and D_m is the mean diameter. A mean diameter D_m, for α-Fe_2O_3 nanoparticles synthesized by $Fe(NO_3)_3{\cdot}9H_2O$ and $FeCl_3{\cdot}6H_2O$ were found ~87 and ~60 nm, respectively.

3.5. Magnetic properties of α-Fe_2O_3 nanoparticles

Magnetic hysteresis measurements for synthesized samples were carried out using vibrating sample magnetometer (VSM) at room temperature and the related magnetic parameters are listed in Table 2. Fig. 7(i) shows the *M–H* curves of the α-Fe_2O_3 nanoparticles at 300 K. It can be seen that the magnetization increases almost linearly under an applied magnetic field up to 5000 Oe. The saturation in the magnetization could not be observed even under the high magnetic field of 17,500 Oe. This observation is similar to the earlier study [27]. The linear increase in the magnetization represents the contribution of the α-Fe_2O_3 antiferromagnetic core [27–28]. When the spin is oriented in anti-parallel directions along *c* axis, as shown in figure [corner of the Fig. 7(i)], the material behaves like a uni-axial antiferromagnet. Fig. 7(ii) shows the hysteresis loop between 0 and 5000 Oe. Hysteretic behavior is the result of surface spin disorder [28].

The observed Ms, Mr and Hc of the α-Fe_2O_3 nanoparticles synthesized by $Fe(NO_3)_3{\cdot}9H_2O$ is larger than that of synthesized by $FeCl_3{\cdot}6H_2O$ as the precursor. It indicates that the magnetization of ferromagnetic materials is sensitive to microstructural characteristics such as size and shape of the crystal structure [29–32].

4. Conclusions

In this report, we have successfully synthesized monodisperse α-Fe_2O_3 nanoparticles by hydrothermal method without using any template or organic surfactant during the synthesis process. This procedure has advantages in producing large-scale nanomaterials for their industrial application. The effects of two different iron precursors on the physical properties of α-Fe_2O_3 nanoparticles have been also investigated. The structural morphology and size of the synthesized nanoparticles were determined using XRD and HR-TEM techniques. The synthesized α-Fe_2O_3 nanoparticles exhibit a weak ferromagnetic behavior at room temperature.

Acknowledgements

MS is thankful to Prof. A.B. Sammadar, Director MNNIT, Allahabad for extending the research fellowship to one more year. AKO is thankful to the Alexander von Humboldt Stiftung for the award of a research fellowship. The Department of Chemistry of MNNIT, Allahabad is gratefully acknowledged for granting access to the available research facilities.

References

[1] R. Wang, Y. Chen, Y. Fu, H. Zhang, C. Kisielowski, J. Phys. Chem. B 109 (2005) 12245.
[2] X. Tenga, H. Yang, J. Mater. Chem. 14 (2004) 774.
[3] S. Laurent, D. Forge, M. Port, A. Roch, C. Robic, L.V. Elst, R.N. Muller, Chem. Rev. 108 (2008) 2064.
[4] K.J. Sreeram, M. Nidhin, B.U. Nair, Colloids surf, B 71 (2009) 260.
[5] H. Zhou, S.S. Wong, ACS Nano 2 (2008) 944.
[6] W. Zhao, H. Chen, Y. Li, L. Li, M. Lang, J. Shi, Adv. Funct. Mater. 18 (2008) 2780.
[7] S. Liu, J. Zhou, L. Zhang, J. Guan, J. Wang, Macromol. Rapid Commun. 27 (2006) 2084.
[8] H. Srivastava, P. Tiwari, A.K. Srivastava, R.V. Nandedkar, J. Appl. Phys 102 (2007) 054303.
[9] H.H. Kung, Transition Metal Oxides: Surface Chemistry and Catalysis, Elsevier, New York, 1989.
[10] L. Huo, W. Li, H. Cui, S. Xi, J. Wang, B. Zhao, Y. Shen, Z. Lu, Chem. Mater. 12 (2000) 790.
[11] P. Chauhan, S. Annapoorni, S.K. Trikha, Thin Solid Films 346 (1999) 266.
[12] M. Fukazawa, H. Matuzaki, K. Hara, Sens. Actuators B 12 (1993) 133.
[13] K.K. Lepers, Vestn. Akad. Nauk. SSSR 4 (1990) 26.
[14] G. Bate, E.D. Wohlforth, Ferromagnetic Material, North-Holland, Amsterdam, The Netherlands, 1980.
[15] R.M. Cornell, U. Schwertmann, The Iron Oxides, Structure, Properties, Reactions, Occurrence and Uses, VCH, Weinhein, 1996.
[16] T. Lindgren, H. Wang, N. Beermann, L. Vayssieres, A. Hagfeldt, S.E. Lindquist, Solar Energy Mater. Solar Cells 71 (2002) 231.
[17] M. Sorescu, R.A. Brand, D.M. Tarabasanu, J. Appl. Phys. 85 (1999) 5546.
[18] K. Byrappa, T. Adschiri, Prog. Cryst. Growth Chem. 53 (2007) 117.
[19] J. Chen, L. Xu, W. Li, X. Gou, Adv. Mater. 17 (2005) 582.
[20] H.P. Klug, L.E. Alexander, X-ray Diffraction Procedure, Wiley Inter Science, New York, 1954, p. 504.
[21] D.L.A. de Faria, S.V. Silva, M.T. de Oliveira, J. Raman Spectrosc. 28 (1997) 873–878.
[22] G. Nasibulin, S. Rackauskas, H. Jiang, Y. Tian, P.R. Mudimela, S.D. Shandakov, L. Nasibulina, J. Sainio, E.I. Kauppinen, Nano Res. 2 (2009) 373.
[23] W. Dong, C. Zhu, J. Mater. Chem. 12 (2002) 1676.
[24] P.L. Casanova, M.M. Scherer, Hyperfine Interact. 174 (2007) 111.
[25] Y.M. Zhao, Y.H. Li, R.Z. Ma, M.J. Roe, D.G. McCartney, Y.Q. Zhu, Small 2 (2006) 422.
[26] L. Maa, L. Kranendonk, W. Cai, Y. Zhao, J. Baba, Aerosol Sci. 40 (2009) 588.
[27] C. Xia, C. Hua, Y. Xiong, N. Wang, J. Alloys Compd. 480 (2009) 970.
[28] M. Tadi, D. Markovi, V. Spasojevi, V. Kusigerski, M. Remskar, J. Pirnat, Z. Jaglici, J. Alloys Compd. 441 (2007) 291.
[29] S.Y. Zeng, K.B. Tang, T.W. Li, J. Colloid Interf. Sci. 312 (2007) 513.
[30] X.M. Liu, S.Y. Fu, H.M. Xiao, C.J. Huang, J. Solid State Chem. 178 (2005) 2798.
[31] S.F. Wang, H.M. Cao, F. Gu, C.Z. Li, G.J. Huang, J. Alloys Compd. 457 (2008) 560.
[32] M. Srivastava, S. Chaubey, A.K. Ojha, Mater. Chem. Phys. 118 (2009) 174.